

DEVELOPMENT OF AN EFFICIENT SOLAR CONCENTRATOR AND UTILIZATION IN COPPER EXTRACTION FROM COPPER MINERALS

K. Yang ^a, Y. Nahmad-Molinari ^{b*}, L.F. Camacho-Conzález ^b, F.M. de los Santos-García ^b, A. López-Valdivieso ^{a*}

^a Universidad Autónoma de San Luis Potosí, Instituto de Metalurgia, San Luis Potosí, Mexico

^b Universidad Autónoma de San Luis Potosí, Instituto de Física, San Luis Potosí, Mexico

(Received 22 February 2024; Accepted 16 December 2024)

Abstract

A novel and cost-effective solar concentrator was developed to enhance efficient copper extraction. Based on the criteria for a stationary compound parabolic concentrator, the reflector geometry incorporates a half-spherical curve and a strength line. This design significantly improves the concentrator's ability to capture more marginal rays than widely used commercial solar concentrators. In this study, a newly configured solar concentrator was constructed with aluminum sheets and tested in San Luis Potosí, Mexico, with a comprehensive performance analysis. The investigation revealed an optical efficiency of 0.73 and a maximum thermal efficiency of 68%. The experimental results demonstrated that the solar collector could absorb solar radiation throughout the year without a tracking system. It efficiently facilitated the copper sulfide ore leaching process at a medium temperature of approximately 70 °C. Capital cost analysis indicated an exceptionally low unit manufacturing cost of only \$ USD 125/m². The study further proposes that the implementation of this solar collector could potentially double the copper recovery rate and triple the annual increase in copper cement without contributing to CO₂ emissions. Additionally, the feasibility of deploying this new concentrator on an industrial scale was thoroughly evaluated to provide substantial support for the further development of clean copper production technology through further innovation.

Keywords: Solar energy; Net-zero carbon emissions; Compound parabolic collectors; Acid leaching; Copper recovery

1. Introduction

Excessive CO₂ emissions represent a critical global environmental challenge, necessitating a 45% reduction by 2030 in order to achieve net-zero emissions by 2050, as outlined in the Paris Agreement [1]. In 2020, a significant movement for net-zero carbon emissions emerged, urging governments to demonstrate genuine commitment to carbon neutrality. Subsequent studies proposed essential engineering frameworks for reducing rare-metal costs and mitigating the harmful environmental impacts of natural gas hydration and drilling [2-4]. Reducing CO₂ emissions from the industrial sector is imperative, given its 25% share of global annual emissions and 37% of global fossil fuel consumption in 2022 [5]. Solar technology has emerged as a promising alternative to fossil fuels, with substantial developments aimed at reducing CO₂ emissions.

Integrating solar technologies into the production process of energy-intensive industries is appealing. Recent investigations into stationary compound

parabolic concentrators (CPC) have evaluated their performance, efficiency, and costs, demonstrating the efficiency achievable with these concentrators while concurrently reducing costs [6, 7]. Similarly, Ahmadi et al. designed a solar concentrator with a flat bottom and parabolic-curved sides that achieved an optical efficiency of 0.8 at a manufacturing cost of \$250 [8]. Martin explored the use of 3D-printing technology to reduce the CPC costs to \$490, significantly lower than those of commercial counterparts [9]. Most concentrators, as observed in previous research, adopt parabolic profiles for their reflector geometry, which often require precise manufacturing processes and result in higher costs.

Copper, a major industrial metal, is experiencing continuous growth in demand. Low-grade copper sulfide ores, including chalcocite (Cu₂S) and covellite (CuS), account for 90% of total copper production. In hydrometallurgy, which constitutes 20% of primary copper production, a copper concentrate is obtained by [10, 11]. This concentrate is then processed at high temperatures to extract copper from the mineral. An

Corresponding authors: yuri@ifisica.uaslp.mx *; alopez@uaslp.mx **



alternative process, leaching, offers advantages over pyrometallurgical techniques by avoiding SO_2 gas emissions and enabling the direct conversion of dissolved copper into metallic copper [12]. However, copper sulfides exhibit slow leaching kinetics at 25 °C, so high-temperature leaching is required to improve the process [13, 14]. Despite the benefits of solar thermal collectors (STC) in reducing energy consumption and CO_2 emissions during leaching processes, their adoption is hindered by high investment costs. The capital cost of STC with a thermal storage system range from USD 5000/kW to USD 10500/kW, compared to USD 3000-8400/kW for coal plants [15]. Consequently, the attractiveness of solar collectors is diminished by the substantial increase in capital costs. This study aims to design an economical, efficient, and easily manufacturable STC to enhance copper recovery in extraction processes. The focus is on the utilization of solar energy for the leaching of secondary copper sulfides by employing a novel solar concentrator design to convert solar radiation into heat for the agitation copper leaching process.

2. Design of a new solar thermal concentrator

Solar concentrators are categorized into imaging and non-imaging forming systems, depending on whether the sun's rays are focused within a point, a focus line, or neither. The parabolic trough concentrator (PTC), concentrating solar rays to its focus, is widely acknowledged as the most mature and commercialized thermal technology, extensively employed in high-temperature industrial processes. However, its reflector geometry limits the acceptance to solar rays within a specific narrow angle, necessitating a tracking system to enhance efficiency, thereby incurring additional capital costs. Another trough-type technology, the Compound Parabolic Concentrator (CPC), utilizes a reflector formed by

combining two symmetrical parabolic segments with different focal lengths. This geometric profile efficiently concentrates solar rays to a wide aperture within an acceptance angle, allowing CPCs to operate without a continuous tracking system and achieving higher thermal efficiency. Studies indicate that it can attain temperatures between 60-150 °C for most industrial processes with medium-temperature requirements, making CPC suitable for the expected operating range of 50-80 °C in leaching processes [16].

Traditional CPC always adopts the parabolic reflector geometry and the Cartesian ovoid, which are theoretically perfect focalizing surfaces for the production of lenses. However, these geometries present challenges in the manufacturing processes and result in high costs. In 2016, the successful application of the Five-hundred-meter Aperture Spherical radio Telescope (FAST) demonstrated that a spherical surface used as a focalizing surface could substitute the parabolic shape at lower costs [17]. Figure 1 illustrates the geometry of the concentrator, with its configurations during the summer and the winter solstices.

2.1. Material and method

In this work, a half-spherical curve is used as the reflector geometry, inspired by the spherical surface of FAST. To illustrate the reflection of rays in the concentrator, representative cases are selected for the incident solar rays at noon during the summer and winter solstices. In Figure 1a, when the sun is directly over above the Tropic of Cancer at noon on the summer solstice, the sector ADE represents the paraxial zone, reflecting all incident rays within this sector to point C, forming a caustic line. Figure 1b illustrates solar rays concentrating most directly on the Tropic of Capricorn at noon during the winter solstice. The paraxial zone shifts from sector ADE to

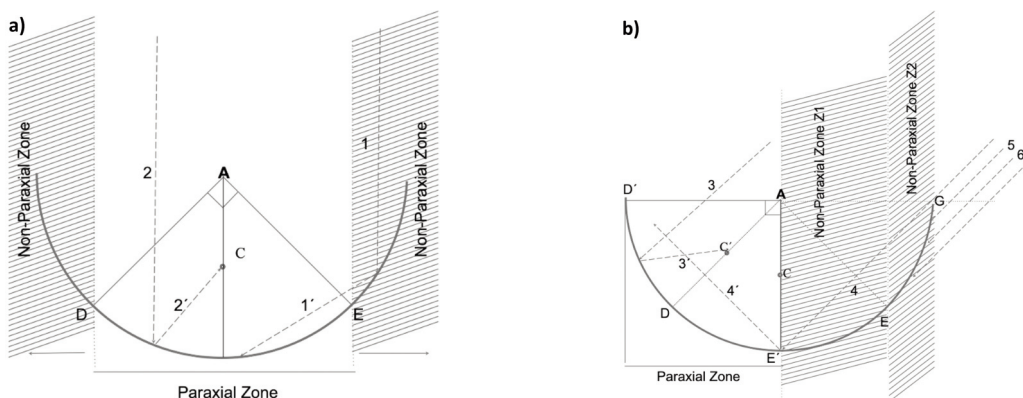


Figure 1. Geometry of the concentrator: (a) on summer solstice and (b) on winter solstice

sector AD'E', reflecting incident rays within this sector to point C'. Figure 2 demonstrates that the sector AD'E overlaps with the ADE and AD'E' sectors as the Sun moves from the Tropic of Cancer to the Tropic of Capricorn. This overlap indicates that all incident rays within sector AD'E are reflected to the vicinity of points C and C'. Consequently, the heat receiver can be positioned from point C to point C' to receive solar rays consistently from spring to winter without positional changes.

The arc EG on the right-hand side of the half-spherical curve in Figure 2 is replaced by a straight in EF. This modification offers two advantages: 1) The line EF is easier and more cost-effective to manufacture compared to the arc EG; 2) While the arc EG in Figure 2a tends to shed a significant amount of the incident rays, the line EF in Figure 2b has the advantage of capturing the most marginal ray.

The angle (θ) formed between the line EF and the

of the materials used in the collector. The optical efficiency is calculated using the formula [18]:

$$\eta_{optical} = \tau_1 \tau_2^{(n)} \alpha (1-L) \Gamma \tag{1}$$

where τ_1 and τ_2 are the transmittance of the outer envelope of the heat receiver and the reflectivity of the concentrator surface respectively, (n) is the average number of reflections, α is the absorptance of the coating surface, L is any geometric loss due to the gap between the heat receiver and the concentrator, and Γ is the fraction of the incident solar radiation accepted by the concentrator after correction for "loss of diffuse". The optical losses include geometric, reflection and absorption losses.

All parameters are listed in Table 2. The τ_1 , τ_2 , α and (n) are provided by the material suppliers. Γ is characterized by the geometrical concentration ratio C_{geom} . An ideal low-concentration collector should be

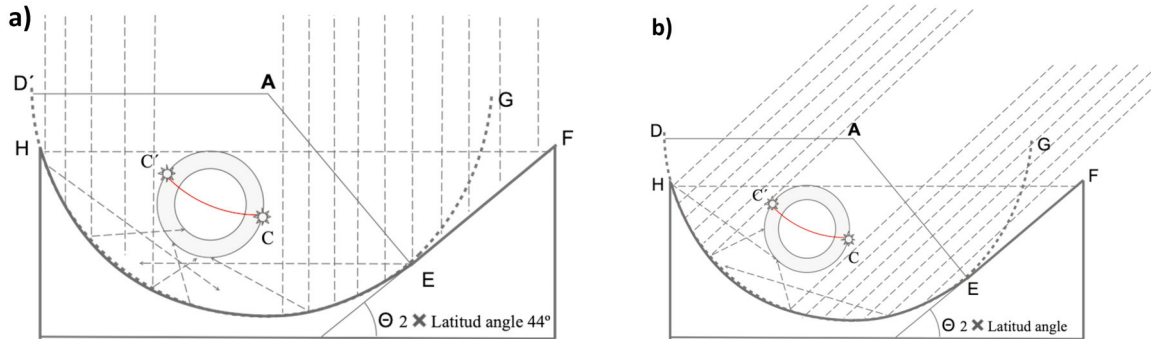


Figure 2. Illustration of ray tracing for the concentrator: (a) on summer solstice and (b) on winter solstice

horizon is twice the latitude angle of 22.1°. This implies that during spring and winter, when the sun's path is within this wedge, a substantial portion of the direct solar radiation can be efficiently collected.

In accordance with the function involving the acceptance angle (θ_c) and geometrical concentration ratio (C_{geom}), the calculated C_{geom} should be 1.43x [18]. The acceptance angle of this concentrator (θ_c) measures 44.2°, equivalent to twice the latitude angle. Other geometric sizes are listed in Table 1.

In addition to the acceptance angle $\pm\theta_c$, the optical performance is further characterized by the optical efficiency. In practical applications, the value can be roughly estimated from the performance parameters

Table 1. Geometry of the new concentrator

| Parameters | Dimension (m) |
|--|---------------|
| Width of the collector | 0.22 |
| Length of the collector | 1.8 |
| Height of the collector | 0.1 |
| Curvature radius of the half-spherical curve | 0.1 |

able to gather about $1/C_{geom}$ of the diffuse insolation [18]. If a typical diffuse fraction is assumed to be 12%, Γ is estimated as follows:

$$\Gamma = 88\% + 12\% * \frac{1}{C_{geom}} \tag{2}$$

Where the direct isolation fraction is 88%, Γ is estimated as 0.97 at $C_{geom} \cong 1.43x$

The geometric loss L is given by:

$$L \cong \frac{g}{\pi r} \tag{3}$$

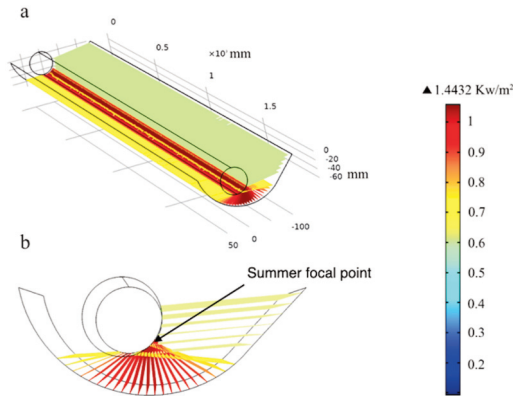
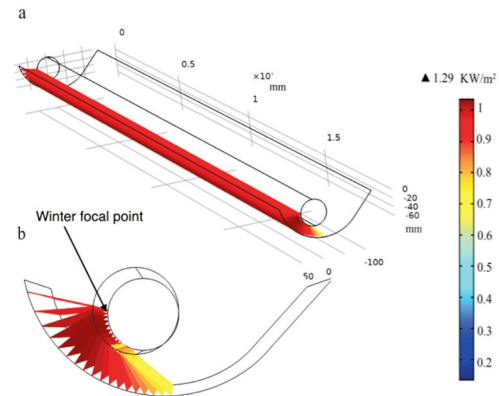
Where g represents a gap between the reflector and the absorber surface and r is an absorber radius. As a result, the optical efficiency $\eta_{optical}$ of our newly designed concentrator is 0.73.

A numerical simulation was conducted using COMSOL Multiphysics to investigate the concentration performance of the new concentrator throughout the year without any tracking system. The



Table 2. Performance parameters for concentrator

| Parameter | symbol | Value |
|--|-------------------------|--------------|
| Transmittance of outer envelope of the heat receiver (polycarbonate) | τ_1 | 0.9 |
| The reflectivity of the concentrator surface (Alumina) | τ_2 | 0.95 |
| Average number of reflections | (n) | 0.8 |
| Absorptance of coating surface | α | 0.95 |
| Gap loss | L | 0.076 (Eq.3) |
| Correction for loss of diffuse | Γ | 0.97 |
| Optical efficiency | η_{optical} | 0.73 (Eq.1) |

**Figure 3.** (a) Solar flux distribution on the absorber surface and (b) cross-section on summer solstice (20/7/2023)**Figure 4.** (a) Solar flux distribution on the absorber surface and (b) cross-section on winter solstice (21/12/2023)

15th day of each month, excluding February, July, September, and December was randomly selected as the focus of the simulation. The solar flux distribution on the surface of the heat receiver predominantly relies on the daily solar irradiation, geometric properties of the concentrator, and thermophysical properties of the heat receiver.

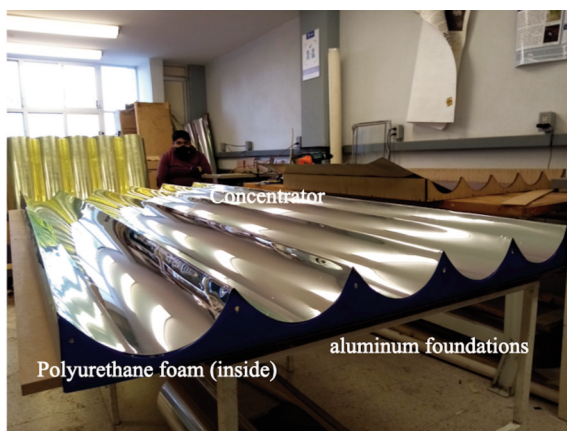
COMSOL has the capability to automatically adjust the sun's geographic location based on a specified day or hour. Assuming a solar peak irradiation of 1 kW/m^2 , 105 solar rays are randomly directed towards the tube at various times during

different seasons. The distributions of solar flux on the tube's surface during the summer and winter solstices are obtained and illustrated in Figure 3 and Figure 4. In Figure 3, the maximum energy flow reaches 1.44 kW/m^2 at the summer focal point, which corresponds to a 44% increase in energy input. Calculably, the tube receives few rays, and the focal point shifts from the right side to the left as the solar incident angle decreases during the day of the winter solstice. Consequently, the maximum energy flow at the winter focal point is 1.29 kW/m^2 , whereby the collector increases the energy input by 29%.

The new concentrators are made of aluminum sheets (0.3 mm thickness, 40 Brinell hardness), as depicted in Figure 5. Aluminum foundations support them, utilizing the same material as the concentrators. The aluminum foundations are filled with polyurethane foam to minimize heat loss between the concentrator and the floor.

2.2. Laboratory setup

Copper minerals with a total copper grade of 1.45%, of which 53.79% was secondary copper sulfide, were sourced from a mine in Mexico. The particle size ranged from 40-250 μm . The lixiviant, holding 3 L water, 0.23 kg ferric sulfate (19.5w Fe^{3+}), and 26 ml acid sulfate (95%-98%w), was heated to 50

**Figure 5.** The new concentrator

°C, 60 °C, and 70 °C, respectively. A 1.16 kg sample was added in suspension to the lixiviant and stirred for 2h (the solid-to-liquid ratio of the slurry is 0.4). The initial concentration of Fe^{3+} and H^+ in the aqueous solution was 15g/L. Ten milliliters of slurry was extracted after 3 min, 5 min, 10 min, 20 min, 30 min, 45 min, 60 min, 90 min, and 120 min, respectively. The liquid samples were filtered and diluted for assay. All solid samples were filtered, cleaned, dried, and prepared for Cu^{2+} assay.

Blackened aluminum tubes were utilized as receivers instead of glass evacuated tubes to prevent breakage during installation, as illustrated in Figure 6. To ensure optical accuracy, the black tubes were fixed in the vicinity of points C and C' by plastic plates, as shown in Figure 2. The collectors were sealed with polycarbonate covers, and the air trapped between the tube and the cover formed a greenhouse effect, reducing conductive and convective heat losses. The water tank volume expanded to 1000 L with a 25m² solar collector area. All PVC pipes used in the system were wrapped with polyurethane.

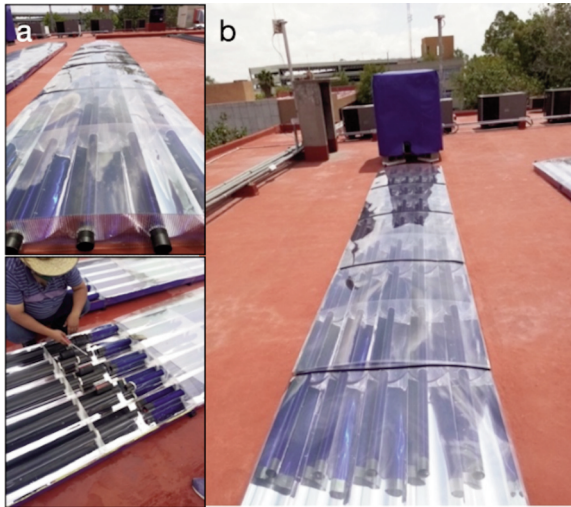


Figure 6. New solar collector (a) Overall and internal structure of collector; (b) Water tank and collector

2.3. Optical and thermal experiments

The test was conducted on the roof of a building of the Universidad Autónoma de San Luis Potosí, Mexico. The experiments were conducted from 9:00 to 18:00, with cold water drained from the tank and circulated through the collector. An ambient temperature sensor was placed in a shelter above the ground and shielded from direct insolation. All temperature data from the thermometers were acquired every 10 seconds. A pyranometer (CM22, Kipp&Zonen, ±5%) and a pyrhemometer (CHIP,

Kipp&Zonen, ±5%) were placed on the aperture area of the CPC to measure the global solar irradiation (G_g) and the direct normal irradiation (G_{DN}), respectively. The solar irradiation that entered the concentrator's aperture area (G_{cpc}) was calculated through Eq. 4-7 [19]:

$$G_{cpc} = G_{dp} + G_d \quad (4)$$

$$G_{dp} = G_{DN} \times \cos(\theta) \quad (5)$$

$$G_d = (G_g - G_{dp}) / C_{geom} \quad (\text{if } (\beta + \theta_A) < 90^\circ) \quad (6)$$

where G_{dp} and G_d are the direct and the diffuse solar irradiations entering the CPC trough aperture area, W/m², G_g global solar irradiation and G_{DN} the direct normal irradiation. geometrical concentration ratio, θ_A is the incidence angle, β is the tilt angle of the CPC, 23.5°. Correspondently, the incidence angle θ is estimated by the following expression (for a south facing, tilted surface in the Northern Hemisphere):

$$\cos(\theta) = \sin(La - \beta)\sin\delta + \cos(L - \beta)\cos(\delta)\cos(h) \quad (7)$$

where, L is the latitude, 23.5°, δ is the solar declination, and h is the hour angle (negative-east, positive-west). The incident angle is retrieved from the National Renewable Energy Laboratory Solar Position Algorithm platform (SPA) [20].

Considering that on equinox days the sun moves within the acceptance angle of the concentrator throughout the day due to the transversal projection of the incidence angle on that day, it is inferred that the concentration performance during equinox days is better than that on solstice days. Given that the solar irradiation in March is the highest, the spring equinox day is selected to investigate optical and thermal performances.

3. Performance tests of the new solar concentrator

3.1. Optical performance

The measured values for global solar irradiation (G_g), direct normal irradiation (G_{cpc}), and solar irradiation entering the concentrator's aperture area (G_{cpc}) are presented in Figure 7. G_g fluctuates between 400-1000 W/m², while G_{DN} ranges between 300-600 W/m². Consequently, the solar irradiation entering the concentrator's aperture area (G_{cpc}), calculated using Eqs. 4-6, falls within the range of 200-700 W/m². This indicates that approximately 50%-70% of G_g is effectively collected. The G_{cpc} curve remains higher than the G_{DN} curve between 9:00 and 16:00, showcasing the concentrator's ability to gather about

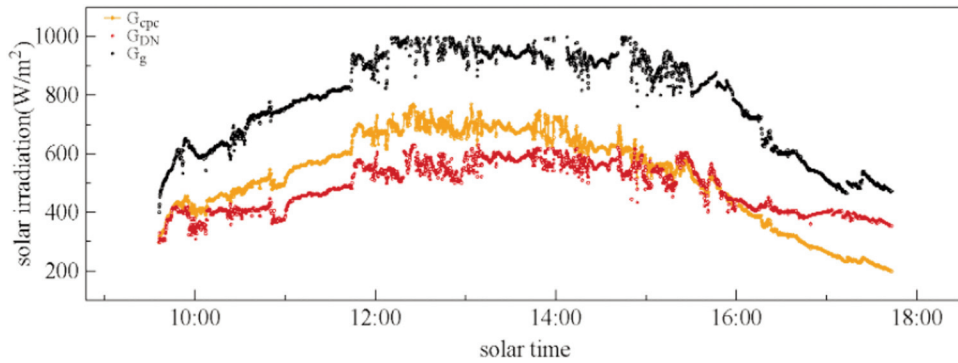


Figure 7. Solar irradiation within a daily test in San Luis Potosi, Mexico on March 20, 2023

$1/C_{geom}$ of the diffuse insolation. However, after 16:00, the G_{cpc} curve descends below the G_{DN} curve, indicating that the cessation of direct solar radiation collection as the sun moves outside the acceptance angle.

3.2. Thermal performance

The thermal experiments began on March 20 at 8:00 a.m. and lasted until March 23, at 6:00 p.m., i.e. for a continuous duration of 32 hours. The pump was activated at 8:00 a.m. and deactivated at 3:00 p.m. Subsequently, the pump was restarted, and the water was heated up again at 10:30 a.m. the following day. A thermometer (PT 1000) with a measuring error of $\pm 0.1^\circ\text{K}$ was strategically placed in the tank to monitor the water temperature. Data logging was done every 10 seconds to record the water temperature.

The water temperature gradually increased from 25°C to 83°C at 14:00, followed by a gradual decrease at 3:00 p.m., indicating that the heat output surpassed input during this period. Consequently, the temperature naturally decreased from 80°C to 70°C

at 10:30 a.m. the next day. Subsequently, the temperature then began to rise again when the pump was restarted, reaching a maximum of 92°C at 14:30. This observation indicates superior thermal efficiency and insulation of the testing system when the pump was turned off.

The instantaneous thermal efficiency of the solar collector was calculated using Eq. 8 below:

$$\eta_{thermal} = \frac{T_{water} - T_{ambient}}{G_g} \quad (8)$$

Where T_{water} is the water temperature in the storage tank and $T_{ambient}$ is the ambient temperature. According to the measured results in Figure 8, it can be found that the maximum thermal efficiency $\eta_{thermal}$ is 68% and the average value is 42%.

4. Copper sulfide ore leaching

4.1. Material and method

Minera Rio Tinto, a small copper mine in Chihuahua, Mexico, possesses copper ores with a

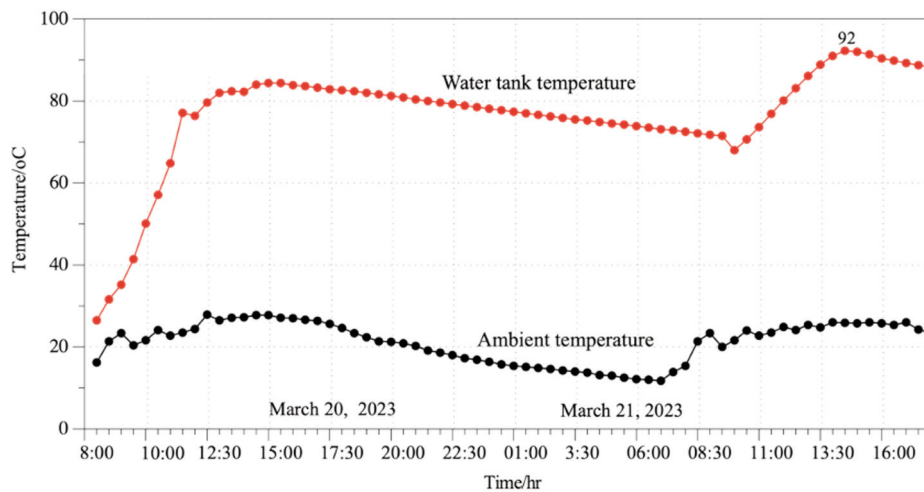


Figure 8. Water temperature change as a function of solar time in San Luis Potosi, Mexico

total grade of 1.45% Cu and an acid-soluble copper grade of 1.42%. Following the current milling circuit, the particle size varies from 40-250 μ m. The elemental chemical assay of the ore is presented in Table 3. It indicates that copper exists in different forms: 21.38% as copper sulfate (CuSO_4), 22.76% as copper oxide (CuO and Cu_2O copper mineral species), 53.79% as secondary copper sulfide (Cu_2S and CuS), and 2.07% as primary copper sulfide (CuFeS_2 and Cu_3FeS_4).

coating on pyrite particles (FeS_2), within cracks in pyrite particles, coated with iron hydroxide (HFeO_2), kyanite (Al_2SiO_5), and other mineral structures. Additionally, Bornite (Cu_3FeS_4), chalcocopyrite (CuFeS_2), and copper sulfate (CuSO_4) were also identified in the sample, along with some non-stoichiometric sulfate ($\text{Cu}_x\text{S}_y\text{O}_z$). The choice of agitation leaching in this mine is based on the mineralogy of the ore body, the topography of the

Table 3. Chemical composition of the copper sulfide ore sample

| | Mineral | | | | | Total |
|----------------|-------------------------|-------------------------------|--------------|--------------------------|------------------------|-------|
| | Copper soluble in water | Copper soluble in acetic acid | Copper oxide | Secondary copper sulfide | Primary Copper sulfide | |
| Ore assay % | 0.026 | 0.284 | 0.33 | 0.78 | 0.03 | 1.45 |
| Distribution % | 1.79 | 19.59 | 22.76 | 53.79 | 2.07 | 100 |

A scanning electron microscope (SEM-EDS, JSM-6610LV, JEOL) was employed for the analysis of mineral species in the ore and the copper species remaining in the residue. The chemical analysis of the samples was conducted using an atomic absorption spectrophotometer (AAS), specifically a Perkin Elmer 3110.

The results of the ore before leaching are depicted in Figure 9. The analysis revealed the presence of Cu_2S in various forms within the ore, including

mine site, and the current economic conditions.

4.2. Leaching process experiments and results discussion

The leaching experiments were conducted in a leaching tank where 1.16 kg of the sample was kept in suspension with the lixiviant by mechanically agitating the slurry. The lixiviant consisted of 3 L distilled water (with a solid-to-liquid ratio of 0.4),

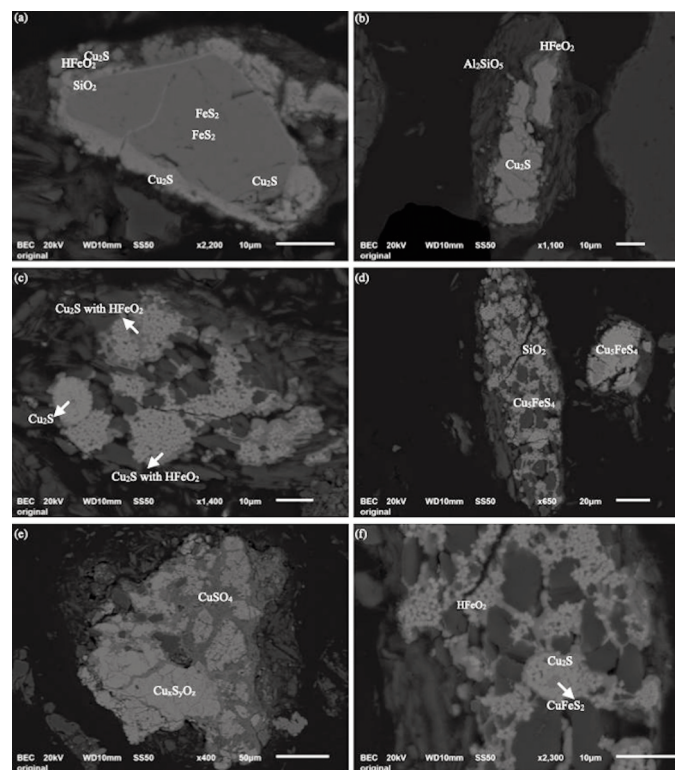


Figure 9. SEM-EDS photomicrographs of copper ore before leaching

Table 4. Cu recovery in different leaching temperature

| Time(min) | 3 | 5 | 10 | 20 | 30 | 45 | 60 | 90 | 120 |
|-------------|-------------------|------|------|------|------|------|------|------|------|
| Temperature | Cu extraction (%) | | | | | | | | |
| 25 °C | 14.7 | 16.8 | 25.2 | 35.4 | 44 | 45.8 | 53.3 | 51.1 | 51.8 |
| 50 °C | 16.7 | 19.8 | 27.2 | 45.2 | 51.6 | 55.5 | 63.1 | 71.3 | 75.4 |
| 60 °C | 20.7 | 25.9 | 35.8 | 52.2 | 60.5 | 65.7 | 74.3 | 79.8 | 83.7 |
| 70 °C | 30.5 | 35.6 | 40.6 | 56.7 | 66.5 | 78.5 | 85.5 | 85.9 | 91.5 |

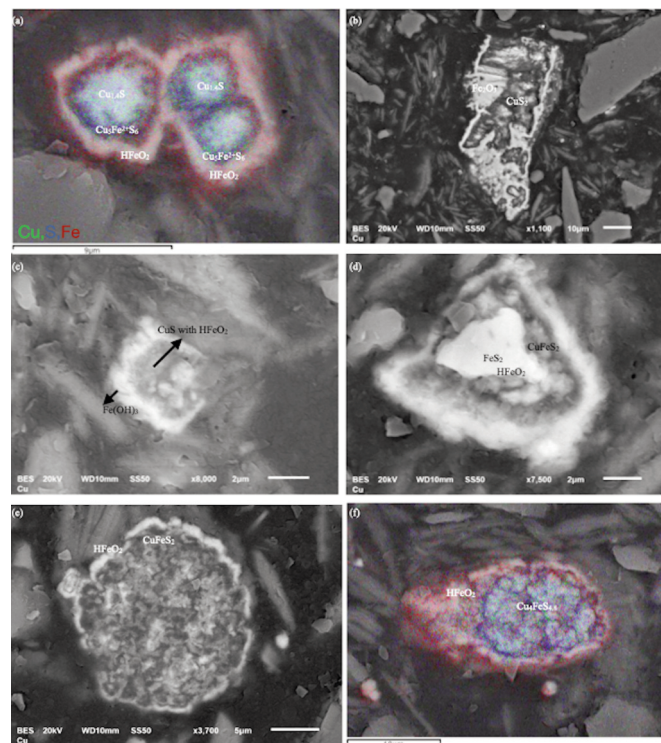
0.23 kg ferric sulfate ($\text{Fe}_3\text{SO}_4 \cdot x\text{H}_2\text{O}$; 19.5% Fe^{3+}), and 26 ml sulfuric acid (95%-98%w) from J.T. Baker. The initial concentration of Fe^{3+} and H^+ in the aqueous solution was 15 g/L. A 10 ml slurry sample was withdrawn from the tank at 3, 5, 10, 30, 45, 60, 90, and 120 min. The liquid samples were filtered and diluted for assay. All solid samples were filtered, cleaned, dried, and prepared for Cu^{2+} assay.

The effects of leaching temperature on copper recovery were investigated in a laboratory setup. The results in Table 4 demonstrated that the temperature variation significantly enhances Cu recovery. At 70 °C, 56.7% of the copper was extracted in the first 20 min and eventually exceeded 91% after 120 min, while only 35.4% copper recovery was achieved in 20 min and 51.8% in 120 min at ambient temperature. The new solar collector can easily supply a high leaching temperature, significantly improving the efficiency of copper extraction compared to the process at ambient temperature. Thus, 70 °C meets the

temperature requirement for the Cu leaching process, which is expected to operate within a temperature range of 50-80 °C.

The leaching residue at 70 °C, were examined by SEM-XRD, as shown in Figure 10. It was found that the CuSO_4 and the non-stoichiometric copper sulfides were completely leached. Moreover, the copper left in the residues remained as CuS , $\text{Cu}_{1.4}\text{S}$, FeS_2 , as well as some primary copper sulfides, as shown in Fig.10(a) and (b), Cu_2S was not leached or was only partially leached to $\text{Cu}_{1.4}\text{S}$, as the Cu_2S fully encapsulated in iron oxide and pyrite.

The layer of iron oxide and pyrite prevented the lixiviant from diffusing to the surface of the CuS , which suppressed the oxidation of CuS to Cu^{2+} . Bornite (Cu_5FeS_4) was also detected, as shown in Fig.10(f). Cu_5FeS_4 is the oxidation product of chalcopyrite (CuFeS_2), therefore, it was difficult for CuFeS_2 to react completely with H_2SO_4 and Fe^{3+} , even at 70 °C.

**Figure 10.** SEM photomicrographs of leached residue (70 °C)

5. Evaluations of newly designed solar collectors

According to the mineralogy of the ore body, topography of the mine site, and current economic conditions, the agitation leaching is used in Minera Rio Tinto. Agitation leaching is a capital-intensive but very compact technique, in which the ore is suspended in stirring tanks for several hours or days. The 100% of copper recovery can be approached. As of now, the daily ore feeding is 10 tons, and the leaching time is 3 h. The final copper extraction is around 50%, with an annual copper cement production of 26 tons in 2021. The electricity consumption in the agitation leaching process is 1997 MWh based on the power of the water pump and agitator, resulting in 1481 tons of CO₂ emissions.

The solar collector array is intended to be integrated into the existing agitation leaching system. The schematic diagram of the integrated plant is illustrated in Figure 11. The hot water discharged from the solar collectors passes through the spiral heat exchanger to supply the heat needed for leaching. The slurry should remain in the first vat for several hours until its temperature reaches above 70 °C. Additionally, fresh sulfuric acid and ferric sulfate are added to oxidize the slurry. Once the slurry temperature reaches 70 °C and above, it flows upward into the second vat for further leaching. After 2 h, the slurry flows through the filtration. The pregnant leach

solution (PLS) overflows the tank after separation, where the cementation reaction occurs, and the cupric ions convert to copper cements while iron transforms to Fe (II) and Fe (III) ions. The raffinate solution is then pumped back into the first leaching vat to replenish the ferric sulfate.

Minera Rio Tinto is currently leaching copper sulfide ore at ambient temperature. If the leaching temperature were increased in the current process, significant improvements would be evident. Table 5 compares the current leaching route with the new solar-leaching and electric heating routes, highlighting the key changes.

In comparison to the current route, case 1 and case 2 in Table 5 demonstrate that the copper recovery rate after 2 hrs increases from 50% to 91.5% by elevating the leaching temperature from ambient temperature to 70°C. Moreover, the daily ore load increases from 10t to 15 t. The final cathode copper production rises from 26t/a to 73t/a, nearly three times as high as with the current industrial process.

Additionally, the Cu residue after each cycle of leaching in cases 1 and 2 reduces by 50%. In case 2, it is observed that electric consumption increases by 16.7% compared to the new solar energy process in case 1, and CO₂ emissions also increase by 17% due to the electric heater. Thus, the application of the new solar energy in the Cu leaching process is proven to be cost-effective, efficient, and environmentally friendly.

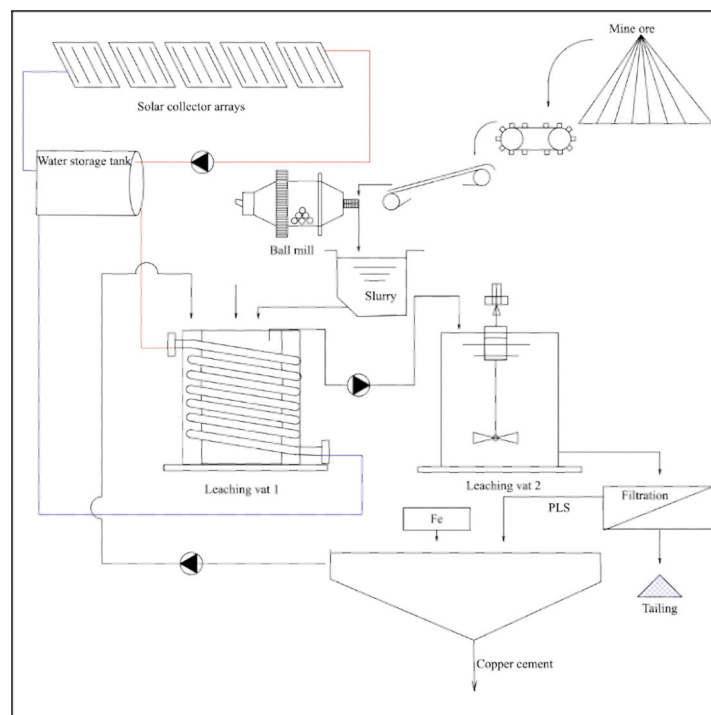


Figure 11. Schematic diagram of the solar agitation leaching operation

Table 5. Comparison among industrial cases of agitation leaching process

| Rio Tinto, Mexico | Current process | Case 1: New process integrated with solar collectors | Case 2: process integrated with electric heater |
|--|---|--|---|
| Operation | | | |
| Cu cement (only leach), t/a | 26 | 73 | 73 |
| H ₂ SO ₄ consumption, t/t Cu | 3.45 | | |
| Ore feed to leach | | | |
| Average Cu grade, % | Cu 1.45(total), Cu 1.42 (acid-soluble), Cu 0.03(acid-insoluble) | | |
| Ore size to leach, um | 80%-174 | | |
| Ore fed to leach, t/d | 10 | 15 | 15 |
| Agitation vats | | | |
| No of vats | | 2 | |
| Impeller power, kW | | 132 | |
| Water pump power, kW | | 48 | |
| No of water pump (Leach only) | | 2 | |
| Electric heater power, kW | - | - | 76 |
| Temperature, °C | ambient | 70 | 70 |
| Leach residue | | | |
| Predominant mineralogy | Major covellite, chalcocite, minor chalcopyrite | Major chalcopyrite, minor covellite | Major covellite, chalcocite, minor chalcopyrite |
| Cu in residue, % | 0.3-0.4 | 0.15-0.17 | 0.15-0.17 |
| Leaching efficiency | | | |
| Cu recovery (leach only), % | 50 | 91.5 | 91.5 |
| Residence time of solids in leach, h | 3 | 2 | 2 |
| Electricity consumption (leach only), MWh/a | 1997 | 1997 | 2663 |
| CO ₂ emission, t/a | 1481 | 1481 | 1975 |

Table 6. Manufacture cost of the CPC collector-array

| Material | Use | Cost per unit \$USD | Units | Cost \$USD |
|---|----------------------|---------------------|--------------------|-------------|
| A CPC collector-array (including 5 CPC-type collector) | | | | |
| Aluminum sheet 3003 | CPC structure | 15 /m ² | 8.16m ² | 122 |
| Polyurethane | Concentrator | 6.75/L | 20L | 135 |
| Copper tube | Heat receiver | 40 c/u | 5 | 200 |
| Polycarbonate plane | Enclosure, supporter | 16.35/m | 3.5m | 57 |
| Tee tube plus 40mm | connection | 1.55c/u | 5 | 7.75 |
| Connection of tube plus | connection | various | various | 20 |
| Tube plus 20mm | connection | 0.75/m | 6.6m | 4.95 |
| connector | | various | various | 10 |
| Stainless Steel T Bolt Clamp | connection | 0.65c/u | 64 | 41.6 |
| Total | | 598 | | |
| A 1000L water tank | | | | |
| Polyethylene water tank | | 80c/u | 1 | 80 |
| Aluminum sheet 3003 | Enclosure | 16.35/m | 3.51 | 57 |
| A thermal system | | | | |
| CPC collector array | | 598 c/u | 5 | 2990 |
| A 1000L water tank | | 137 c/u | 1 | 137 |
| Total | | | | 3127 |
| Payback period | | | | 5.4years |



The economic and environmental advantages offered by solar thermal system make the new solar collector particularly attractive, provided that its capital cost remains reasonable. In this study, the reflector geometry was designed as a half-spherical curve and a strength line, constituting a solar thermal system comprising 25 solar collectors and a 1000 L water tank. The manufacturing costs are itemized and presented in Table 6 for the sake of clarity. A comparison with three other designs from the literature [21], considering optical efficiency and manufacturing cost reveals that their optical efficiency ranged from 0.5 to 0.8, with a unit cost between \$125 and \$490. In contrast, our newly designed collectors boast an optical efficiency of 0.73, as discussed in the previous section. The CPC collector arrays comes at a cost of \$2990 for 25 solar collectors, translating to a remarkably low unit cost of \$119 per collector. The total cost of the system is \$3,127, which includes five solar collector arrays (totaling \$2,990) and a 1000 L water tank priced at \$137, results in a cost of \$125/m².

The payback period is the amount of time it takes for the savings to cover the initial investment. It can be calculated as:

Payback period (P) = initial investment (C₀) ÷ annual savings (C_s)

Based on the energy cost of natural gas in Mexico, the energy produced by the solar thermal system annually (based on solar radiation, collector efficiency, etc.), the payback period of the collector was estimated at approximately 5.4 years. The detailed calculation process is provided in Appendix 2. This cost-effectiveness, coupled with superior optical efficiency, positions the new solar collector as a promising solution for sustainable energy applications.

6. Conclusions and future work

In this study, we have successfully developed an efficient and practical solar concentrator designed for the copper leaching process in copper mines. The newly configured solar concentrator, employing a spherical curve connected with a straight line, was meticulously constructed, evaluated, and subjected to a comprehensive performance analysis. The concentrators have demonstrated the capability to collect solar irradiation all year round without relying on tracking systems. The following conclusions are drawn:

The optical efficiency of our new solar collector reaches 0.73, accompanied by a maximum thermal efficiency of 68%. This new solar thermal collector (STC) proves to be efficient, cost-effective, and easy

to manufacture, contributing to the enhancement of copper recovery in leaching processes.

The newly developed solar collector can generate 1000L of hot water using a 25 m² of solar collector area. It heats the water to 80 °C and maintain it at 70 °C for the subsequent 24 h.

The investigation showcased a novel integrated solar collector with an agitation leaching system, demonstrating significant economic benefits in a case study of leaching production. The unit cost of this new solar collector is a mere USD 119, the entire system is USD 125/m², resulting in a substantial reduction in capital costs.

The integration of the new concentrator into the copper leaching process in a Mexican mining industry would result in a substantial improvement in copper recovery. The recovery rate at 70 °C would increase to 91.5% from 50%, subsequently raising the daily ore load from 10 t to 15 t. The eventual copper cement production would surge from 26 t/a to 73 t/a, nearly three times as much as with current industrial processes. Importantly, CO₂ emissions would remain unchanged. The feasibility of the new concentrators on an industrial scale is conducive to promoting further innovation in cleaner copper production technology.

This study would encourage further studies on more efficient solar concentrators with low costs. We have only considered the manufacturing costs in this study. Further economic analysis such as operating costs, end-of-life costs, and maintenance costs could be investigated. Improving the optical design to increase optical efficiency such as minimizing gap losses, could be explored. Scaling up the laboratory solar collector to a pilot plant is a crucial future application to advance efficient, effective, and carbon neutral copper leaching. Additionally, we plan to study on the cementation process by utilizing a new solar concentrator to transform solar radiation into heat.

Acknowledgments

This work was funded by the project CEMIE-SOL P066 and the National Council for Science and Technology, Mexico (CONACyT). Mineral ores and support from Minera Río Tinto, Chihuahua, México to conduct this work is fully acknowledged.

Appendix 1

The CO₂ emissions can be calculated using equation below:

The carbon dioxide emissions:

$$\text{CO}_2(\text{kg}) = \text{kWh} \cdot 0.742$$



Where, the conversion factor was 0.742 tCO₂/MWh for coal-fired power plants at Mexico [22]. Once obtain the amount of electricity consumed, typically measured in (kWh), multiply the conversion factor to get the total CO₂ emissions.

In the case of not using electric heating, the leaching process employs two water pumps with a power of 48 kW each and one impeller agitator with a power of 132 kW. Assuming the leaching process operates 24 h a day and 365 days a year, the annual power consumption is calculated as 1997 MWh. The corresponding carbon dioxide emissions are calculated based on an emission conversion factor related to electricity consumption.

Appendix 2

Initial cost of the solar thermal system = \$3127 USD

Cost of energy = \$0.027 USD/kWh (2024 natural gas prices of Mexico)

Solar Radiation Availability for San Luis Potosí = 5.6 kWh/m²/day

Average thermal efficiency of the CPC = 0.42

The effective thermal = 0.42 × 5.6 kWh/m²/day × 25 m² = 58.8 kWh/day

Daily Energy saving = (58.8 kWh/day) × (\$0.027 USD/kWh) = \$1.59 USD/day

Payback period = Initial cost of the solar system / Daily Energy saving = \$3127 USD / \$1.59 USD/day = 5.4 years

Abbreviations

CPC, compound parabolic concentrator; **LX**, agitation leaching; **SX**, solvent extraction; **EW**, electrowinning.; **STC**, solar thermal collector; **PTC**, parabolic trough concentrator.

Authors' contributions

Ke Yang: Original draft. Investigation. Formal analysis. Resources. Data Curation. Visualization

Yuri Nahmad Molinari: Validation. Resources. Writing - Review & Editing. Funding acquisition

Luis Fernando Camacho Conzález: Software. Visualization

Fátima MI de los Santos García: Validation.

Alejandro Lopéz Valdivieso: Conceptualization. Methodology. Validation. Writing - Review and Editing. Supervision.

Data availability

Data are available on request to the authors.

Conflict of interest

All authors disclosed no relevant relationships.

Reference

- [1] United Nations Climate Change, Paris Agreement, United Nations, Paris, 2015, p.1-27.
- [2] F. Wang, X. Liu, B. Jiang, H. Zhuo, W. Chen, Y. Chen, X. Li, Low-loading Pt nanoparticles combined with the atomically dispersed FeN(4) sites supported by Fe(SA)-N-C for improved activity and stability towards oxygen reduction reaction/hydrogen evolution reaction in acid and alkaline media, *Journal of Colloid and Interface Science*, 635 (2023) 514-523. <https://doi.org/10.1016/j.jcis.2022.12.160>
- [3] Q. Li, D. Zhao, J. Yin, X. Zhou, Y. Li, P. Chi, Y. Han, U. Ansari, Y. Cheng, Sediment instability caused by gas production from hydrate-bearing sediment in northern South China sea by horizontal wellbore: evolution and mechanism, *Natural Resources Research*, 32 (4) (2023) 1595-1620. <https://doi.org/10.1007/s11053-023-10202-7>
- [4] Q. Li, F. Wang, Y. Wang, C. Zhou, J. Chen, K. Forson, R. Miao, Y. Su, J. Zhang, Effect of reservoir characteristics and chemicals on filtration property of water-based drilling fluid in unconventional reservoir and mechanism disclosure, *Environmental Science and Pollution Research*, 30 (19) (2023) 55034-55043. <https://doi.org/10.1007/s11356-023-26279-9>
- [5] R. Simon, P. Hugues, P. Levi, T. Vass, Industry, The international energy agency (IEA), Paris, 2023.
- [6] C. Jiang, L. Yu, S. Yang, K. Li, J. Wang, P.D. Lund, Y. Zhang, A review of the compound parabolic concentrator (CPC) with a tubular absorber, *Energies*, 13 (3) (2020) 695. <https://doi.org/10.3390/en13030695>
- [7] H.A. Gilani, S. Hoseinzadeh, Techno-economic study of compound parabolic collector in solar water heating system in the northern hemisphere, *Applied Thermal Engineering*, 190 (2021) 116756. <https://doi.org/10.1016/j.applthermaleng.2021.116756>
- [8] A. Ahmadi, M.A. Ehyaei, A. Doustgani, M.E.H. Assad, F. Esmailion, A. Hmida, D.H. Jamali, R. Kumar, Z.X. Li, A. Razmjoo, Recent progress in thermal and optical enhancement of low temperature solar collector, *Energy Systems*, 14 (1) (2023) 1-40. <https://doi.org/10.1007/s12667-021-00473-5>
- [9] M. Martín-Sómer, J. Moreno-SanSegundo, C. Álvarez-Fernández, R. van Grieken, J. Marugán, High-performance low-cost solar collectors for water treatment fabricated with recycled materials, open-source hardware and 3d-printing technologies, *Science of The Total Environment*, 784 (2021) 147119. <https://doi.org/10.1016/j.scitotenv.2021.147119>
- [10] S.S. Jena, S.K. Tripathy, N.R. Mandre, R. Venugopal, S. Farrokhpay, Sustainable use of copper resources: beneficiation of low-grade copper ores, *Minerals*, 12 (5) (2022) 545. <https://doi.org/10.3390/min12050545>
- [11] H.R. Watling, A.D. Elliot, M. Maley, W. van Bronswijk, C. Hunter, Leaching of a low-grade, copper-nickel sulfide ore. 1. Key parameters impacting on Cu recovery during column bioleaching, *Hydrometallurgy*, 97 (3-4) (2009) 204-212. <https://doi.org/10.1016/j.hydromet.2009.03.006>
- [12] G. Ji, Y. Liao, Y. Wu, J. Xi, Q. Liu, A review on the



- research of hydrometallurgical leaching of low-grade complex chalcopyrite, *Journal of Sustainable Metallurgy*, 8 (3) (2022) 964-977. <https://doi.org/10.1007/s40831-022-00561-5>
- [13] S. Javanshir, H. Imantalab, M. Fathi, Accelerating copper leaching from a complex ore containing atacamite: optimisation and kinetic studies, *Canadian Metallurgical Quarterly*, 63 (1) (2024) 1-12. <https://doi.org/10.1080/00084433.2023.2171675>
- [14] K. Pérez, R.I. Jeldres, S. Nieto, E. Salinas-Rodríguez, P. Robles, V. Quezada, J. Hernández-Ávila, N. Toro, Leaching of pure chalcocite in a chloride media using waste water at high temperature, *Metals*, 10 (3) (2020) 384. <https://doi.org/10.3390/met10030384>
- [15] E. Aramendia, P.E. Brockway, P.G. Taylor, J. Norman, Global energy consumption of the mineral mining industry: Exploring the historical perspective and future pathways to 2060, *Global Environmental Change*, 83 (2023) 102745. <https://doi.org/10.1016/j.gloenvcha.2023.102745>
- [16] E. Bellos, D. Korres, C. Tzivanidis, K. Antonopoulos, Design, simulation and optimization of a compound parabolic collector, *Sustainable Energy Technologies and Assessments*, 16 (2016) 53-63. <https://doi.org/10.1016/j.seta.2016.04.005>
- [17] P. Jiang, N.-Y. Tang, L.-G. Hou, M.-T. Liu, M. Krčo, L. Qian, J.-H. Sun, T.-C. Ching, B. Liu, Y. Duan, Y.-L. Yue, H.-Q. Gan, R. Yao, H. Li, G.-F. Pan, D.-J. Yu, H.-F. Liu, D. Li, B. Peng, J. Yan, F. Collaboration, The fundamental performance of FAST with 19-beam receiver at L band, *Research in Astronomy and Astrophysics*, 20 (5) (2020) 064. <https://doi.org/10.1088/1674-4527/20/5/64>
- [18] J. O'Gallagher, *Nonimaging optics in solar energy*, Springer Cham, Illinois, USA, 2008, p.25.
- [19] J.A. Duffie, W.A. Beckman, *Solar engineering of thermal processes*, Wiley, New Jersey, 2013, p.345.
- [20] I. Reda, A. Andreas, Solar position algorithm for solar radiation applications, *Solar Energy*, 76 (5) (2004) 577-589. <https://doi.org/10.1016/j.solener.2003.12.003>
- [21] H. Jannesari, B. Babaei, Optimization of solar assisted heating system for electro-winning process in the copper complex, *Energy*, 158 (2018) 957-966. <https://doi.org/10.1016/j.energy.2018.06.119>
- [22] A. Amellina, Additional information on calculating the emission factor of Mexico for the JCM, Institute for Global Environmental Strategies, Hayama, Japan 2017, p.4. <https://doi.org/10.57405/iges-6346>

RAZVOJ EFIKASNOG SOLARNOG KONCENTRATORA I NJEGOVA PRIMENA U EKSTRAKCIJI BAKRA IZ MINERALA BAKRA

K. Yang ^a, Y. Nahmad-Molinari ^{b*}, L.F. Camacho-Conzález ^b, F.M. de los Santos-García ^b, A. Lopéz-Valdivieso ^{a*}

^a Autonomni univerzitet San Luis Potosi, Institut za metalurgiju, San Luis Potosi, Meksiko

^b Autonomni univerzitet San Luis Potosi, Institut za fiziku, San Luis Potosi, Meksiko

Apstrakt

Razvijen je novi i isplativ solarni koncentrador za poboljšanje efikasnosti ekstrakcije bakra. Na osnovu kriterijuma za stacionarni kompozitni parabolični koncentrador, geometrija reflektora uključuje polusfernu krivu i liniju čvrstoće. Ovaj dizajn značajno poboljšava sposobnost koncentratora da uhvati više marginalnih zraka u poređenju sa komercijalnim solarnim koncentradorima koji su u širokoj upotrebi. U ovom istraživanju, novo-konfigurisani solarni koncentrador je konstruisan od aluminijumskih ploča i testiran u San Luis Potosiju, Meksiko, uz sveobuhvatnu analizu performansi. Istraživanje je pokazalo optičku efikasnost od 0,73 i maksimalnu termalnu efikasnost od 68%. Eksperimentalni rezultati su pokazali da solarni kolektor može apsorbovati sunčevo zračenje tokom cele godine, bez sistema za praćenje. Efikasno je olakšan proces luženja rude bakar sulfida na srednjoj temperaturi od približno 70 °C. Analiza kapitalnih troškova je pokazala izuzetno nisku cenu proizvodnje po jedinici, od samo 125 USD/m². Dalje, studija predlaže da implementacija ovog solarnog kolektora može potencijalno udvostručiti stopu iskorišćenja bakra i utrošiti godišnji porast bakarnog cementa, a bez doprinosa emisiji CO₂. Takođe, izvedena je temeljna procena izvodljivosti primene ovog novog koncentratora na industrijskom nivou kako bi se pružila značajna podrška daljem razvoju tehnologije čiste proizvodnje bakra kroz dalje inovacije.

Ključne reči: Solarna energija; Nulta neto emisija ugljen-dioksida; Kompozitni parabolični kolektori; Luženje kiselinom; Iskorišćenje bakra

